https://doi.org/10.5194/nhess-2020-417
Preprint. Discussion started: 15 January 2021

Natural Hazards and Earth System Sciences
Discussions

Improving flood damage assessments in data scarce areas by retrieval of building characteristics through UAV image segmentation and machine learning – a case study of the 2019 floods in Southern Malawi

Lucas Wouters[1,2], Hans de Moel[1], Marleen C. de Ruiter[1], Anaïs Couasnon[1], Marc J.C. van den Homberg[2], Aklilu Teklesadik[2]

[1]Institute for Environmental studies (IVM), Vrije Universiteit Amsterdam, De Boelelaan 1087, 1081HV Amsterdam
[2]510 , an initiative of the Netherlands Red Cross, Anna van Saksenlaan 50, 2593 HT Den Haag

Correspondence to: Lucas Wouters (wouters.lucas@outlook.com)

Abstract.

Reliable information on building stock and its vulnerability is important for understanding societal exposure to floods. Unfortunately, developing countries have less access to and availability of this information. Therefore, calculations for flood damage assessments have to use the scarce information available, often aggregated on a national or district level. This study aims to improve current assessments of flood damage by extracting individual structural building characteristics and estimate damage based on the buildings' vulnerability. We carry out an Object-Based Image Analysis (OBIA) of high-resolution (11 cm ground sample distance) Unmanned Aerial Vehicle (UAV) imagery to outline shapes. We then use a Support Vector Machine Learning algorithm to classify the delineated buildings. We combine this information with local depth-damage curves to estimate the economic damages for three villages affected by the 2019 January river floods in the Southern Shire basin in Malawi, and compare this to a conventional approach using land use to denote exposure. The flood extent is obtained from satellite imagery (Sentinel-1), and corresponding water depths determined by combining this with elevation data. The estimated damages from the OBIA and aggregated land-use approach yield €10,140 and €15,782, respectively, highlighting the potential for detailed and local damage assessments using UAV imagery.

1. Introduction

Worldwide, flooding is one of the most common and damaging natural hazards in both monetary terms and loss of life (UNDRR, 2019). Estimating flood damage is essential for shaping flood risk management before and disaster management after a flood. This can be done a-priori to support strategic risk reduction, or after an event in order to support recovery. This latter one is knows as a Damage and Needs Assessment (DNA), which is usually based for the most part on ground truth data. For DNAs, household field surveys are conducted, as rapid Damage and Needs Assessments and Post Disaster and Needs Assessments (Jones, 2010). A-priori flood damage assessments are generally modelled and require extensive datasets on flood hazard characteristics, the exposed elements at risk, and the vulnerability of these elements (Budiyono et al., 2015; Alam, A. et al., 2018; UNDRR, 2019). Much work has focused on improving these damage estimates, quantifying the effect of different flood scenarios and its consequences (Murnane et al., 2017). Unfortunately, information on the exposure and vulnerability is often lacking in developing countries or less accessible (M. van den Homberg and Susha, 2018).

https://doi.org/10.5194/nhess-2020-417
Preprint. Discussion started: 15 January 2021


Natural Hazards and Earth System Sciences
Discussions

Therefore, calculations for flood damage assessments have to use the scarce data available, often aggregated on high national or district level. This lack of data complicates accurate and downscaled flood damage assessments (Amirebrahimi et al., 2016; Fekete, 2012). The lower spatial level is, however, required for most flood risk management applications. Building damage, in particular, remains hard to quantify, as this is usually a heterogeneous land-use category. This causes many uncertainties in the assessment about physical structure, content, and flood susceptibility (Wagenaar et al., 2016). Flood damage assessments are a standard procedure to identify economic losses in flood-prone areas, and growing populations and economies have increased the relevance of predicting the impact of impending disasters on the people that live in these areas (Merz et al., 2010). Such assessments can enable the allocation of resources for recovery and reconstruction by humanitarian decision-makers when a disaster does strike (Díaz-Delgado and Gaytán Iniestra, 2014). For example, severe floods in January 2015 have demonstrated the need for improved flood damage assessments in Malawi. During this period, the worst flood disaster in terms of economic damage was recorded for 15 of its 28 districts, predominantly in the Southern Region. The total damage was estimated to be US$ 286.3 million, with the housing sector accounting for almost half of the total damage with US$ 136.4 million (Government of Malawi, 2015). More recently, the Chikwawa district was subjected to extensive flooding because of continuous rainfall by tropical cyclone Desmond in January 2019.

Several studies have suggested that flood damage assessments could be improved by incorporating the vulnerability of building structures. Blanco-Vogt et al., (2015) summarize different methods to retrieve building characteristics and estimate flood vulnerability based on building typologies in a semi-urban environment. Different building parameters are discussed that could affect the building susceptibility to flooding, including height, size, form, roof structure and the topological relation to neighbouring buildings and open space. Typologies are created by taking the remotely sensed data and relating this to potential flood impact. They note that these typologies can be used to link buildings to more detailed damage curves and discuss the challenges in terms of data resolution and techniques in remote sensing. The research of De Angeli et al., (2016) builds on the method of Blanco-Vogt et al., (2015) by developing a flood damage model that differentiates the urban area (using building clusters based on building taxonomies), instead of using a single homogenous land-use class. Remotely sensed data were used to derive exposure and vulnerability information after which it was combined with available building information. The damage was validated, and the model was able to accurately assess damage estimates in an urban setting. Nonetheless, the authors state that a generalization of the procedure needs to be studied further.

Remote sensing has the potential to generate information on the exposure and vulnerability input for damage assessments. Numerous studies have been carried out for mapping land cover, such as built-up areas, with varying methods and spatial scales (Mallupattu and Sreenivasula Reddy, 2013; Ai et al., 2020). With new innovations in the resolution of imagery, also smaller-scale studies can be conducted where remote sensing can be applied to retrieve information on object-level (Klemas, 2015; Englhardt et al., 2019). In a review by De Ruiter et al., (2017) it is stated that common flood vulnerability studies that use land-cover typologies could be improved by incorporating object-based approaches. For example, by developing vulnerability curves for different wall-material types. A technique to derive useful information from remotely sensed image data is Object-Based Image Analysis (OBIA). OBIA has the potential to identify exposed elements and its characteristics accurately when

https://doi.org/10.5194/nhess-2020-417
Preprint. Discussion started: 15 January 2021


Natural Hazards and Earth System Sciences
Discussions

incorporated into a flood damage assessment but there is little literature combining the methods. The process involves grouping pixels into objects based on their spectral properties or external variables, after which they are combined into spatial units for image analysis such as image classification (Blaschke, 2010). Spectral properties to group these objects could, for example, be the mean value or standard deviation of spectral bands of the image. Using this method, instead of a pixel-based classification, over-classification or a 'salt and pepper look' can be avoided as pixels are not defined individually (Blaschke, 2010).

A conventional workflow to conduct an OBIA exists of two major steps: (1) segmentation and (2) feature extraction and classification. The accuracy of this approach is improving with the emergence of higher resolution imagery. More specifically, the literature demonstrates that the relationship between the objects under consideration and the spatial resolution is critical for the accuracy of segmentation and the OBIA in general (Blaschke, 2010; Belgiu and Drăguț, 2014; Xu et al., 2019). Although feature classifications can be done manually, this process would be time-consuming and tedious for large areas. Machine Learning techniques can provide similar results and several statistical methods can be applied that use the information from the designated samples in the classification. Certain techniques exhibit better results than others depending on the case study area, the imagery, or the size of the training set. In a review by Ma et al., (2017) it was concluded, for example, that in the case of land-cover mapping using OBIA, Random Forests and Support Vector Machines perform best in agricultural areas for high-resolution imagery.

From the above it is clear that exposure and vulnerability components are underrepresented in current flood damage assessments, especially in data-scarce areas. In this research, we aim to bridge the gap in data requirement by using automated object recognition and machine learning of high-resolution images. We apply an OBIA to delineate the outlines of buildings and use the machine learning to characterize the buildings. After which classification of building types can be made to implement stage-dependent damage curves based on building material and floodwater characteristics. Remotely sensed images are collected by Unmanned Aerial Vehicle (UAV) that can reach key areas, and the approach is applied to three villages in a flood-prone district in the Lower Shire basin in Malawi. By comparing this method to a conventional land-use based approach using aggregated exposure data, recommendations can be made for future assessments.

2. Data and methods

This research has been divided into three parts following the general procedure of a flood damage assessment (Merz et al., 2010; de Moel and Aerts, 2011; Jongman et al., 2012). Flood risk is defined as a combination of the elements: hazard (flood extent and depth), exposure (exposed assets) and the conditions of vulnerability that are present (the susceptibility of buildings to floods) (UNDRR, 2019). The first part deals with the classifications of elements by creating house typologies by combining information from an Object-Based Image Analysis (OBIA) of high-resolution UAV imagery with a field survey. The second part focusses on analyzing the detected building exposure and assessing the corresponding vulnerability of the objects. In the final part, the data from the steps mentioned above is related to the flood impact corresponding to a specific flood event in the case study area. Based on Sentinel-1 satellite imagery, a flood extent is created, and its related water depth is estimated. The

https://doi.org/10.5194/nhess-2020-417
Preprint. Discussion started: 15 January 2021

Natural Hazards and Earth System Sciences
Discussions
Open Access
EGU

economic damage of the elements is calculated using local building-specific stage-damage curves. We evaluate the influence of building size, water depth and damage curve on our damage assessment model using a one-at-a-time sensitivity analysis, as applied in Ke et al. (2012).

120

To assess the added value of using UAV data on flood damage assessments, the information from an OBIA conducted on high-resolution optical imagery was incorporated into an flood damage assessment and compared to a convential assessment based on disaggregated census data and homogenous land-use pixels. For the conventional damage assessment, building stock information was extracted from the Malawi National Statistical
125 Office (NSO) and used to create corresponding stage-damage curves (Malawi Statistical Office, 2017). This process will from now on be referred to as the *'pixel-based'* approach. Our proposed damage assessment combines the information from an OBIA with local data on building stock to calculate structural damages based on the mid-January 2019 flood. This process will from now on, be referred to as the *'object-based'* approach. The two different models share similarities on the impact of the specific flood event but are inherently different in their
130 approach on the classification of elements and their flood susceptibility. In the terminology of the UNDRR, (2019), this translates into different input data for the exposure and vulnerability components. The sensitivy of the damage parameters are analysed to determine the most influencing factors in the flood damage assessment models. Figure 1 visualizes the method.

135 There is no specific empirical damage data available for the area covered by the UAV imagery. However, the Red Cross and Red Crescent Societies issued an Emergency Plan of Action (EPoA) after the 2019 January river floods in Malawi. Based on preliminary assessment by volunteers on the ground, one of the most affected Traditional Authorities is Makhuwira with a total of 2,434 collapsed houses. In Chikwawa, a total of of 15,974 people were affected, 3,154 houses damaged or destroyed, and 5,078 people reported to be displaced across at least seven
140 camps set up by communities and government. Most of the affected houses were semi-permanent structures (IFRC, 2019), which are also common in our study area.

https://doi.org/10.5194/nhess-2020-417
Preprint. Discussion started: 15 January 2021

Natural Hazards and Earth System Sciences
Discussions

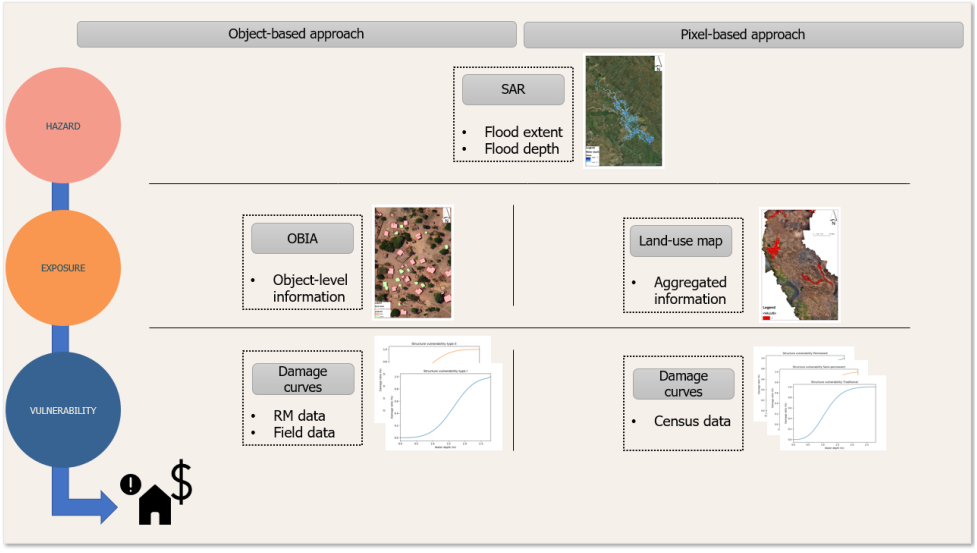

Figure 1. Workflow of the two approaches of flood damage estimation. The left panel shows the object-based approach and the right panel shows the pixel-based approach. Abbreviations: Synthetic-aperture radar (SAR), Object-Based Image Analysis (OBIA), Remote Sensing (RM). The inundation (hazard) map is shown on © Google Satellite. The OBIA and land-use map are created using UAV imagery from the Malawi Red Cross Society.

2.1 Input data

UAV optical imagery was collected in November 2018 by The Netherlands Red Cross (NLRC) and the Malawi Red Cross Society (MRCS) for mapping and flood simulation purposes in the Lower Shire Basin. van den Homberg et al. (2020) give an extensive description of the UAV data collection and UAV used. A Digital Surface Model (DSM) was generated using the collected imagery. Other remote sensing data were acquired from open-source databases, including the Shuttle Radar Topography Mission (SRTM) DEM collected by NASA and the SAR Sentinel-1 imagery collected by Copernicus (Farr & Kobrick, 2000). The High-Resolution Settlement Layer (HRSL) provides an estimate of the settlement extent and population density and was developed by the Connectivity lab at Facebook in combination with the Centre for International Earth Science Information Network (CIESIN) by using computer vision techniques to qualify optical satellite data with a resolution of 0.5m (CIESIN, 2016). The OpenStreetMap (OSM) contains a features layer of manually delineated objects and was used for validation purposes (© OpenStreetMap contributors, 2019). Table 1 summarizes the various datasets.

Table 1: Available datasets in this research. Abbreviations: : Digital Elevation Model (DEM), Digtital Surface Model (DSM), Ground Range Detected (GRD), Malawi Red Cross Society (MRCS), OpenStreetMap (OSM), Shuttle Radar Topography Mission (SRTM) Synthetic-aperture radar (SAR).

	Dataset	Type	Resolution (horizontal)	Data repository	Acquisition
Remote sensing					

https://doi.org/10.5194/nhess-2020-417
Preprint. Discussion started: 15 January 2021

Natural Hazards and Earth System Sciences
Discussions

	HRSL	Land cover	30m	CIESIN	2016
	Satellite	DEM	30m	SRTM, Earth Explorer	Unknown
	Sentinel-1 (GRD)	SAR	23m	Copernicus Scihub	24-01-2019
	UAV	Optical	0.11m	MRCS	11-2018
	UAV	DSM	0.25m	MRCS	11-2018
Geospatial data					
	OSM	Vector	Object	OpenStreetMap	n/a

165

2.1.1 Field survey

To gain information about the building stock present in the case study area, Teule et al. (2019) conducted a field survey on structures and their material in 4 villages in, or surrounding, Traditional Authority Makhuwira, including Jana, Nyambala and Nyangu (Fig. 2). In total, 50 buildings were sampled and used as representative
170 buildings in estimating the susceptibility of building material types in the area. Fig. 3 shows an example. The survey collected characteristics of potential flood vulnerability parameters, including size, height, roof material, wall material, and inventory of the house.

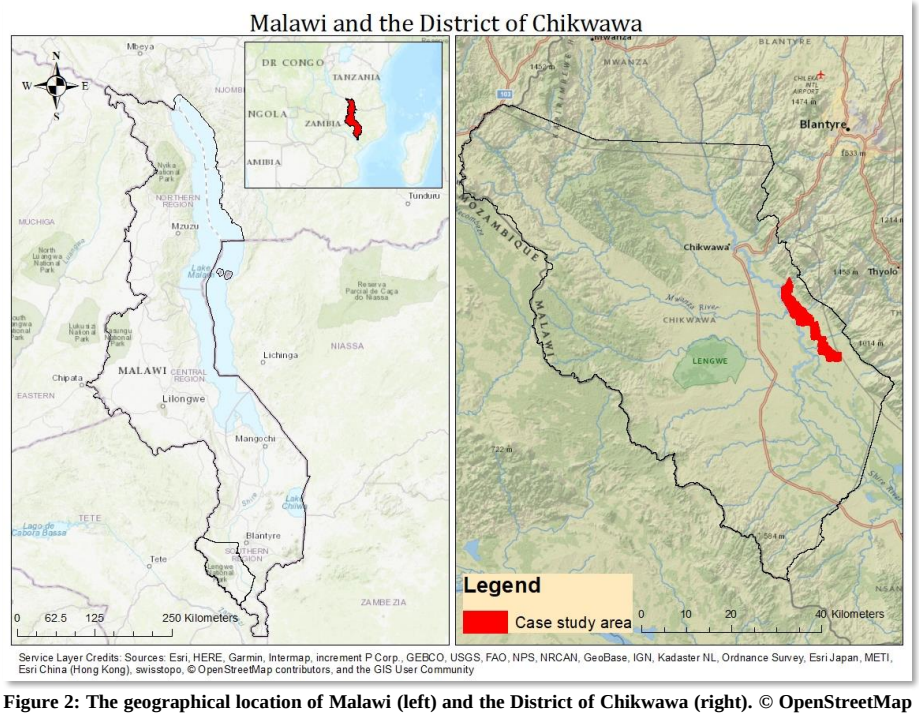

Figure 2: The geographical location of Malawi (left) and the District of Chikwawa (right). © OpenStreetMap contributors, 2019. Distributed under a Creative Commons BY-SA License.

https://doi.org/10.5194/nhess-2020-417
Preprint. Discussion started: 15 January 2021

Natural Hazards and Earth System Sciences
Discussions

Figure 3: Image from one of the sample buildings taken in the case study area (Teule et al., 2019) A clear contrast between building material is visible between the two structures: hatched roofs and unburnt bricks versus iron sheeted roofs and burnt bricks.

2.2 Object-Based Image Analysis (OBIA)

The OBIA consisted of the following steps. First, validation and training samples were collected from the villages in the case study area by manually delineating objects. We manually delineated a total of 144 building to serve as training and 556 as validation. This step was followed by segmenting the high-resolution imagery and classifying the vectorized objects. We selected the open-source geo-software Orfeo Toolbox (OTB). This toolbox is a library for image processing initiated by the CNES (French Space Agency) that includes numerous algorithms created for the purpose of segmentation and classification (Grizonnet et al., 2017). Further development of the toolbox is underway.

Segmentation was performed using the Mean Shift Clustering algorithm utilized by OTB. The mean-shift algorithm exploited by Orfeo relates to the work of Michel et al., (2015), in which the goal of image segmentation is to partition large images into semantically meaningful regions. The following parameters were set: (1) the spatial radius or the neighborhood distance was set to 1.5m; (2) the range expressed in radiometry unit in the multispectral space to 5m; and (3) the minimum size of a region in segmentation 5m² in relation to minimum building sizes. The Support Vector Machine (SVM) algorithm from the same Orfeo library served to classify the vectorized objects from the segmentation. The SVM is a kernel-based machine learning algorithm that has been effectively used to classify remotely sensed data (Mountrakis et al., 2011). The classifier was trained on samples that represented the common features in the selected images and are summarized in Table 2. An example of the output of this process is shown in Fig. 4.

https://doi.org/10.5194/nhess-2020-417
Preprint. Discussion started: 15 January 2021

Natural Hazards and Earth System Sciences
Discussions

Table 2: Samples used as input for training the SVM classifier with mean value ranges of the spectral bands (nm).

Value	Label	Samples	Mean B0	Mean B1	Mean B2
1	Vegetation	28	121-164	135-165	101-136
2	Metal	27	207-241	207-244	205-245
3	Thatch	31	225-241	201-228	184-213
4	Bare	34	171-220	155-197	145-197
5	Shadow	24	113-154	114-150	113-137

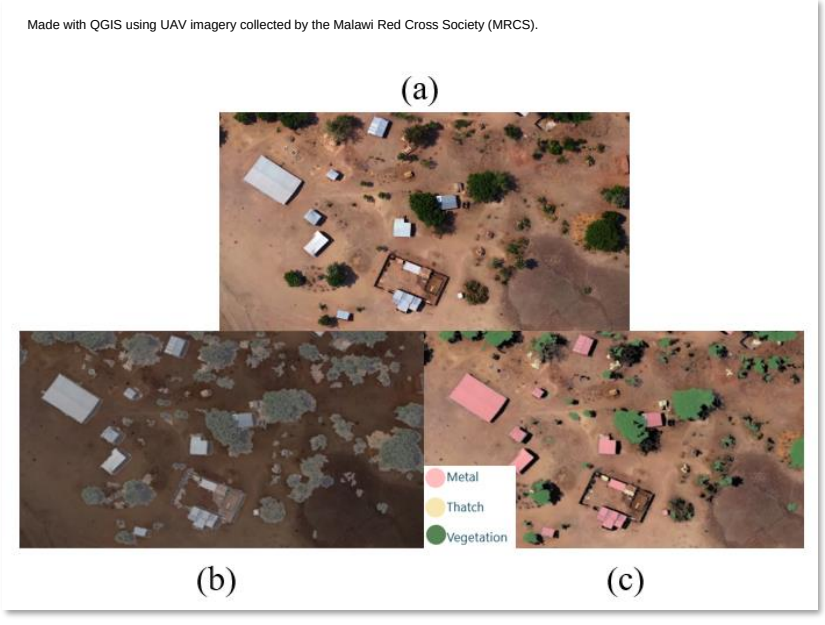

Figure 4: Steps of the OBIA: (a) Original UAV imagery, (b) result of mean-shift segmentation, (c) classification using SVM classifier. The image contains UAV imagery collected by the Malawi Red Cross Society (MRCS), collected in November 2018.

After the segmented objects were classified, a filtering process was conducted in which objects were removed based on their respective height and category. By keeping the two categories that represent buildings with a height over 0.5 m, buildings can be extracted, and potential misses are excluded from the damage calculation. This height was chosen as a value between the height of the ground and a one-story building. The mean height from the DSM was added to the objects by creating centric points of each segment and extracting the elevation values to these points from the UAV DSM map. To derive the height of these objects, a baseline DEM was constructed and subtracted from the mean DSM value. For this, the cells classified as 'Metal'and 'Thatch' were removed from the DEM. Next, ground reference points were placed using visual interpretation to make sure no bushes or trees were selected. The elevation of these ground reference points were correspondingly used to interpolate an elevation surface using IDW (inverse distance weighting) and the elevation of this interpolated surface was used to determine the height of the 'Metal' and 'Thatch' cells by determining the difference with the original DEM elevation.

https://doi.org/10.5194/nhess-2020-417
Preprint. Discussion started: 15 January 2021


Natural Hazards and Earth System Sciences
Discussions

To evaluate the performance of the OBIA model, a map with 556 manually detected reference objects was compared to a map with predicted buildings from the classification. For this purpose, a confusion matrix was created where a prediction can be either a True Positive (*TP*), False Positive (*FP*), True Negative (*TN*), or False Negative (*FN*). In which, *TP* (True Positive) is the number of cases detected both manually and with the automatic approach. FP (False Positive) is the number of cases detected by the automatic approach but not manually. *TN* (True Negative) is the number of cases detected manually but not by the automatic approach. FN (False Negative) is the number of undetected cases. The statistical parameters that were used to test the classification performance are the accuracy, F1-Score, and the Cohen Kappa. The overall accuracy (A) was calculated given Eq. (1):

$$A = \frac{TP + TN}{TP + FP + TN + FN} \quad \textbf{(1)}$$

To test the classification performance per class, the F1-Score was used. This statistic is the weighted mean of both Precision (P) and Recall (R), where 0 indicated the lowest possible score and 1 a perfect score. The parameters are calculated with the following equations:

$$R = \frac{TP}{TP + FN} \quad \textbf{(2)}$$

$$P = \frac{TP}{TP + FP} \quad \textbf{(3)}$$

$$F1 - Score = 2 * \frac{P * R}{P + R} \quad \textbf{(4)}$$

To evaluate the building area, predicted buildings were chosen that have partial or complete overlap with the reference buildings. From this selection, the Relative Error (RE) was calculated per building typology. In this case, the absolute error is normalized by dividing it by the magnitude of the actual value. The RE is calculated through the following expression:

$$RE = \frac{\sum_{n=1}^{N} |\theta^{\wedge} - \theta i|}{\sum_{i=1}^{N} |\theta i|} \quad \textbf{(5)}$$

Where $\theta^{\wedge}$ is the predicted value and θi is the actual value and N is the sample size.

2.3 Flood hazard calculation

To represent the flood hazard, we derive water depths from the January 2019 flood event. This approach takes the following three main steps: (1) extracting SAR data and processing it using SNAP software (SNAP, 2019) to create a flood extent map, (2) preparation of the data in ArcGIS and (3) using the available SRTM DEM to estimate the water surface elevation and extracting the flood water depth.

https://doi.org/10.5194/nhess-2020-417
Preprint. Discussion started: 15 January 2021

Natural Hazards and Earth System Sciences
Discussions

In the first step, pre-processing of the data was performed through calibration and speckle filtering. Post-processing was conducted by geometric correction using the terrain correction function. As the pixel values in SAR imagery can be related to the radar backscatter of the area where it was taken, calibration is necessary to transform the pixels from the digital values recorded by the satellite into backscatter coefficients. This process creates a new product with calibrated values of the backscatter coefficient. The derived product underwent additional speckle filtering to remove the noise from the image using the 'Lee filter'. In the binarization process, water and non-water are separated throughsetting a threshold by analyzing the backscatter coefficient histogram and manually determining the peak characteristics of land and water areas. After this process, flooded areas could be determined by setting a threshold value of 0.0022 which was defined based on the historgram plot of pixel values for reflectivity.

The next step was to prepare the image in ArcGIS. The water was vectorized using the 'Raster to vector' tool and aggregated with the 'Aggregate polygons' tool based on a neighborhood of 100 meters. Single-pixel polygons were removed to exclude noise from the flood map. Any empty spaces in the polygon were filled using the 'Union' and 'Dissolve' tools. These filled spaces can be the result of beneath-vegetation flood areas (Shen et al., 2019) that can be missed by the SAR processing (Shen et al., 2019). They are removed in the next, final step if they are a result of actual topographic factors, such as local hills.

The final step in this approach follows the research of Cian et al., (2018) and S. Cohen et al., (2018), where the flood boundaries along the water surface are used to estimate the elevation of the water surface. The boundaries of the derived flood extent were turned into points with the 'raster to point' tool, after which the elevation values were extracted from the DEM. The water surface was then computed using the 'Inverse Distance Weighting (IDW)' tool from ArcGIS. Essentially, this means that pixels inside of the flood extent get the elevation value of the closest elevation points along the boundary. The water depth can then be calculated by deducting the initial DEM values from the assigned water surface values.

To evaluate the the water depth interpolation method, the result is compared with a flood hazard map obtained from running a hydraulic model that was run for a subsection of the Shire river in a study by Copier et al., (2019). The model was run using Hydrologic Engineering Center's River Analysis System (HEC-RAS) software (Hydrologic Engineering Center, 1998). The Root Mean Square Error (RMSE) is used to compare the different models using the UAV DSM (Cohen et al., 2018).

2.4 Damage estimation

To estimate the damage for the pixel-based approach, the built-up area will be estimated by taking the built-up area of the pixel according to average density percentages and building sizes. This data will be collected by visual interpretation of the UAV imagery. The damage is calculated through the following expression:

$$D_{\mathrm{p}}[€] = \sum_{i=1}^{3} damage(i_{\mathrm{p}}) * a(i_{\mathrm{p}}) * r(i_{\mathrm{p}}) * rc(i_{\mathrm{p}})[€] \quad \textbf{(6)}$$

https://doi.org/10.5194/nhess-2020-417
Preprint. Discussion started: 15 January 2021

Natural Hazards and Earth System Sciences
Discussions

Where:

- i_p = the building typology as determined by the building stock description of the Malawi National Statistical Office (2018);
- $damage(i_p)$ is the damage per pixel in euros calculated with the adjusted stage-damage curve, and using as input the water depth [m] in the considered pixel;
- $a(i_p)$ is the size of the object in area m²;
- $r(i)$ is the ratio of the typology according to the national survey;
- $rc(i)$ is the replacement cost per m² based on the typology (i). These estimates are collected through interviews and focus group discussions in the case study area (Teule et al., 2019).

For the object-based approach the damage can be calculated through the following expression:

$$D_o[€] = \sum_{i=1}^{2} damage(i_o) * a(i_o) * rc(i_o)[€] \quad (7)$$

Where:

- i_o = the building typology as determined by the OBIA and field survey;
- $damage(i_o)$ is the damage per object in euros calculated with the adjusted stage-damage curve, and using as input the water depth [m] in the considered object;

Based on the building typologies found in both the national and our local survey, damage curves were constructed by aggregating the curves from the CAPRA library and adjusting them with the information from Maiti (2007). We follow Maiti (2007), in assuming that that structures constructed with a mud wall tend to collapse at a water depth of 1 meter.

For the pixel-based approach, the description in fourth Integrated Household Survey 2016-2017 (IHS4) of traditional, semi-permanent and permanent buildings is used to aggregate the material-specific damage curves from the CAPRA library. This means, for example, that that the materials used to describe a traditional building are used to construct the curve, being: unfired mud brick, grass thatching for roofs or rough poles for roof beams (Malawi Statistical Office, 2017). The distribution of these three building types in Chikwawa, found in the IHS4, are used to calculate the damage for a flooded pixel. For the object-based approach, the results from the field survey are used to create damage curves for the building typologies determined by aerial observation and the OBIA. In this case, the local distribution found in buildings materials is used to aggregate the curves from the CAPRA library based on percentages.

To quantify how the damage parameters can influence the damage estimate, a one-at-a-time sensitivity analysis will be conducted by increasing and decreasing the different damage parameters with the mean of the respective relative errors. The sensitivity value (SV) will be used to represent the sensitivity and can be calculated by dividing the largest resulting damage by the smallest resulting damage (Koks et al., 2015).

https://doi.org/10.5194/nhess-2020-417
Preprint. Discussion started: 15 January 2021

Natural Hazards and Earth System Sciences
Discussions

3 Results

3.1 Field observations

As a result of the information collected through the building survey, structures are grouped into two types. This is based on the similarity of their flood vulnerability and their distinctive aerial features. A total of 50 samples was taken to represent building stock. No buildings were found that have a wall structuring resembling wood, reed or concrete. In addition, no structures were found having tiles or any other material as the roof, nor any having more than two levels.

3.1.1 Metal-roofs

The first type is composed of burnt and, in a small number of cases (10%), unburnt bricks. This type is less vulnerable to flooding compared to the other type due to its material being less susceptibility to building failure. Its main distinctive aerial feature is a metal sheet roof, but the results of the OBIA and the field survey also indicate that this type of building is often larger than thatch-roofed buildings.

3.1.2 Thatch-roofs

The second type is generally composed of less formal building material, with its main distinctive feature being a thatch roof. The results of the survey seem to indicate a relatively equal distribution between the buildings materials, but as unburnt bricks and mud walls are more susceptible to building failure, this type is considered more vulnerable to flooding.

3.2 Damage curves and maximum damage functions

Two damage curves are created for the object-based approach based on typologies corresponding with the field survey and three for the typologies in the building stock description of the national survey that are used in the pixel-based approach (Fig. 5).

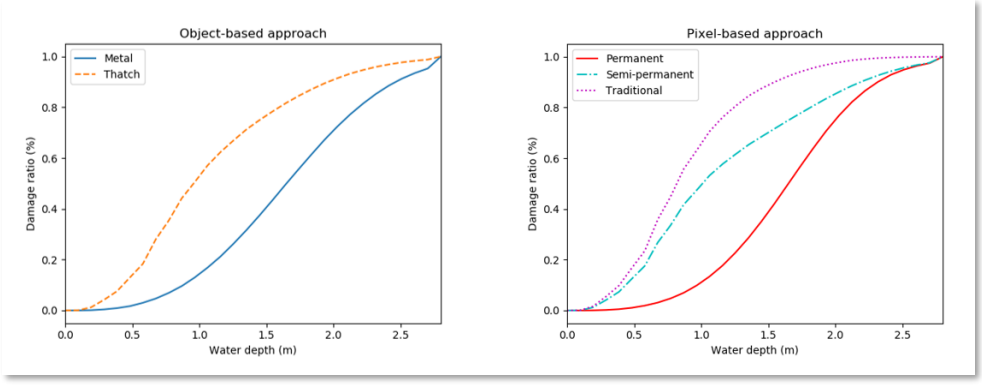

Figure 5: Constructed damage curves for the two typologies derived from field and aerial observation (left-hand panel), and three typologies derived from the description of building stock at district level (right-hand panel) (Malawi National Statistical Office, 2017). The water depth is the flood water relative to the ground floor.

https://doi.org/10.5194/nhess-2020-417
Preprint. Discussion started: 15 January 2021


Natural Hazards and Earth System Sciences
Discussions

The maximum damage values per square meters can be found in Table 3. These values are estimated based on the different kind of materials and the costs of building the structure in Southern Malawi and were validated by local authorities

Table 3: Estimated maximum damage values per m² based on local knowledge of replacement costs (Teule et al., 2019).

Typology	€/m²
Permanent	15.20
Semi-permanent	10.60
Traditional	4.40
Metal-roofed	13.00
Thatch-roofed	9.70

3.3 Flood inundation

The average water depth from the flood event at the case study location was 1.17 meter for the surface water interpolation and 1.22 meter for the hydraulic model run using the UAV DSM (Copier ref). The maximum estimated water depth for both approaches was about 3 meter (3.30 and 2.79 meters, respectively). The RMSE was calculated to be 0.73 meters. The results show that for a flood depth of approximately 3 meters, the surface water interpolation method deviated from the hydraulic model by <0.75 meters on average.

The same method for the total case study area with the SRTM DEM produced a water depth map with an average water depth of 1.26 meter and a maximum water depth of 7 meters (Fig. 6). Objects in the inundated area were assigned the water depth in the corresponding cell.

https://doi.org/10.5194/nhess-2020-417
Preprint. Discussion started: 15 January 2021

Natural Hazards and Earth System Sciences
Discussions

365

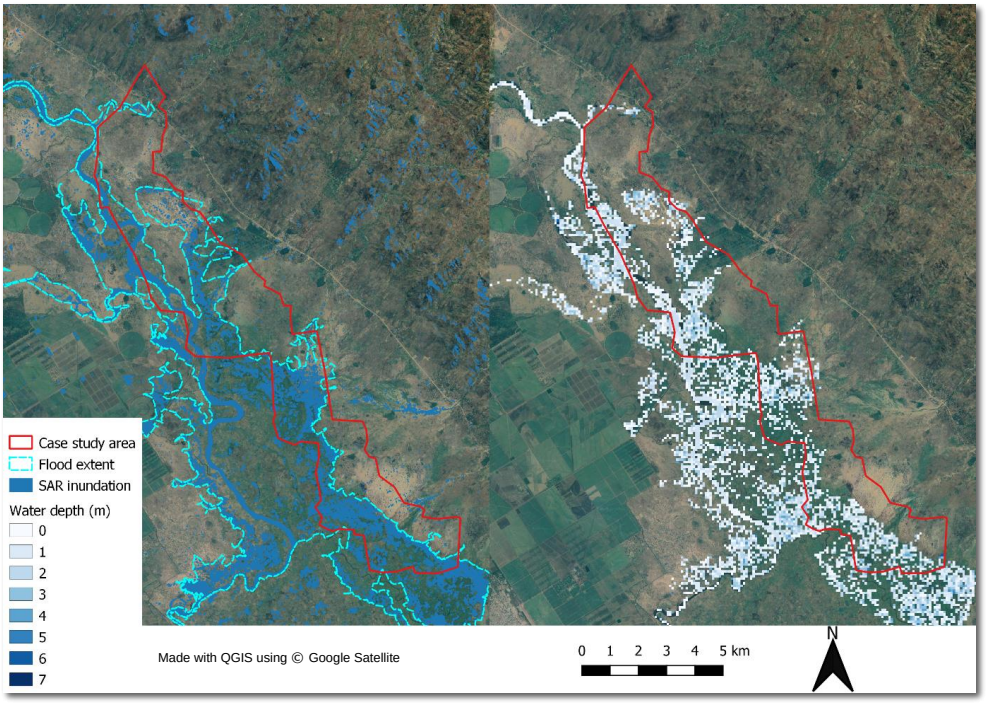

Figure 6: The flood inundation extent for the case study area using the SRTM DEM (left) and the derived water depth map using surface water interpolation (right). The inundation maps are shown on © Google Satellite.

3.4 OBIA quality assessment

370 The implementation of the OBIA model had a varying degree of success according to the statistical tests. Table 4 shows that classification is more reliable for classifiers that have a clear spectral difference with surrounding elements, such as shadow and metal roofs, whereas bare ground and thatched roofs are less easy to distinguish. These spectral difference resulted in a higher F1-Score for buildings with a metal roof (89%) compared to those with a thatched roof (53%). With the F1-score being the harmonic mean of the Precision and Recall, this metric
375 captures both the false negatives and the false positives of the classification proces. The lower F1-score for detected thatch roofs could be attributed to their tendency to blend in with the environment because of their relatively similar spectral properties. With the addition of the height threshold for objects, the individual F1-scores for buildings were improved to 90% for metal-roofed buildings and 72% for thatched-roofed buildings. The increased F1-score for thatched-roof buildings indicates that having additional and accurate information on the
380 height of the objects has a large effect on the individual classification accuracy. The overall accuracy of the initial run shows a value of 77.45%, indicating the amount of correctly classified objects out of the total amount of samples. This value also increases up to 80% with the addition of a height threshold for objects, though this increase is also partly due to the exclusion of poorly performing classes such as ‘Bare ground’.

https://doi.org/10.5194/nhess-2020-417
Preprint. Discussion started: 15 January 2021

Natural Hazards and Earth System Sciences
Discussions

Table 4: Evaluation of the performance accuracy of the OBIA classification. *addition of height threshold by subtracting the extracted DSM and DEM values.

Label	F1-score	F1-score*	Accuracy (%)	Accuracy (%)*
Vegetation	0.91	-		
Metal	0.89	0.90		
Thatch	0.53	0.72	77.45	80.19%
Bare ground	0.49	-		
Shadow	0.90	-		

The building objects from the OBIA are a direct result of the segmentation process, and the relative error seems to reflect the same pattern as the classification process. This means that buildings with a thatch roof tend to be harder to detect because the model groups pixels together that represent different objects, such as bare ground and the thatch roof. For both typologies, the relative error between observed and predicted building area can be observed in Figure. 7. For the thatch roof buildings, 50% of the predictions are found with RE lower than 30%. For the metal-roofed buildings, this same percentage of predictions are found with a RE lower than 7.5%. Generally, metal-roofed buildings tend to be larger in size than thatch-roofed buildings, with a mean building size of 39 m² and 21 m², respectively. For both typologies, the RE tends to decrease as building size increases. This seems to be in line with literature where it is stated that if objects get closer to the size of the available spatial resolution, errors are more likely to occur (Blaschke, 2010).

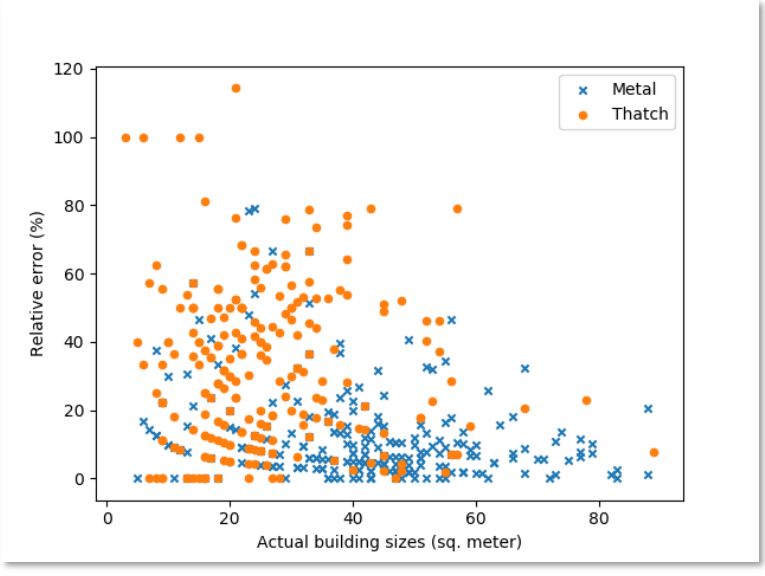

Figure 7: Building area and relative error for both typologies (metal and thatch) in the case study area.

3.5 Damage estimates

By overlaying the separate components of the flood damage assessment, the estimated damages were calculated for both approaches. Compared to a conventional pixel-based approach, the object-based approach provides a

https://doi.org/10.5194/nhess-2020-417
Preprint. Discussion started: 15 January 2021

lower estimation of the exposed built-up area, of about two-thirds (Table 5). As a result, this influences the resulting damage. The flooded built-up area for the land-use based approach and the object-based approach was estimated at 2,541 m² and 3,952 m², respectively. This resulted in estimated flood damage of approximately €10,140 and €15,728, respectively (Table 5).

Table 5: Flooded buildings and built-up area according to (1) the object-based approach, (2) pixel-based approach and (3) the available OSM map, and area and total damage according to (1) the object-based approach, (2) pixel-based approach.

Villages	Number of flooded buildings			Flooded built-up area (m2)			Total damage (€)	
	Object	Pixel	OSM	Object	Pixel	OSM	Object	Pixel
1	9	11	10	371	338	348	1,286	1,754
2	54	92	61	1,424	2,768	1,321	6,215	10,043
3	21	28	26	746	846	732	2,639	3,931
Total	84	132	97	2,541	3,952	2,401	10,140	15,728

Although building densities and average buildings sizes were extracted from the same UAV imagery, a difference can be observed in the flooded built-up area between the two approaches. This is likely a result of the inability of land-use pixels to account for spatial variability of the buildings objects inside a certain area. Similar research on German flood events exemplifies that significant uncertainties are present in flood damage assessments due to information lacking on the number of flooded buildings and the distribution of building use within the flooded area (Merz et al., 2004).

3.6 Sensitivity analysis

By varying the building size and water depth parameters with the mean of the respective relative errors, the sensitivity of the damage parameters for both approaches were estimated. As there is no information on the uncertainty of the damage curve values from the Evaluación de Riesgos Naturales (ERN) database, the influence of this parameter is derived by using only the lowest and highest damage curve from the building types. For example, the lower damage bound for the damage curve sensitivity value in the object-based approach is computed by using only the Metal damage curve and the higher bound using the Thatch damage curve. Table 6 shows that the largest variance in resulting damage is caused by this variance of the damage curves.

Table 6: The sensitivity values (SV) of the different damage parameters for the pixel- and object-based approach.

	Pixel-based	***Object-based***
Parameter	**SV**	
Building size	1.43	1.21
Water depth	1.46	1.56
Damage curve	1.71	1.9

https://doi.org/10.5194/nhess-2020-417
Preprint. Discussion started: 15 January 2021

Similar results have been found by Ke et al., (2012) in an urban flood damage assessment, where the damage function has the largest influential degree of damage followed by the value of the elements at risk. Another study by de Moel et al., (2012) also notes that the most influential parameter in the uncertainty of flood damage estimates is the shape of the depth-damage curves. It can be observed that the parameters involved in flood damage estimation include an amount of uncertainty, and this propagates in the total estimated damage. As the hazard component in both calculations remained equal, the differences can be attributed to the sensitivity of the damage parameters on the building types and damage curve parameters. Moreover, it can be observed that the sensitivity value of building size is lower in the object-based approach compared to the pixel-based approach, which can be attributed to less uncertainty in total building area that is flooded.

4 Discussion

Although this research has uncovered several important factors in the estimation of flood damage based on building detection, the issue deserves further additional research. First, the method was created for a specific case study area with little variation in building types. Building extraction is herein limited to the available data source. For urban areas, classification confusion might occur due to the heterogeneity of building types and structural properties. This complication could yield more uncertainties in assigning appropriate damage curves to buildings, especially as large discrepancies in potential flood damage exist between urban and rural areas in developing countries (Englhardt et al., 2019). Another distinction should be made between when studying areas with river-floods or flash-floods, as capturing the latter with Earth Observation data becomes a challenging task due to the frequency SAR acquisitions can be made (Mouratidis & Sarti, 2013).

The second aspect refers to the additional field survey. The acquired samples provide insight into the relations between the local elements and the remotely sensed characteristics. However, a larger number of samples would be necessary to provide a statistically sound justification of the assumption on this relation. Obtaining field observations could become a difficult task if the method is scaled up, but a promising line of research could be the implementation of services like Mapillary or Google Street View for this purpose. Combining the findings from this kind of research with field surveys can, therefore, complement the conventional methods by aggregating accurate estimates on building sizes, density, and characteristics. This would decrease the amount of uncertainty incorporated in potential scaled-up assessments. The HRSL provides an impressive first glance at exposed settlements and can be used as a base layer to project the distributions of building exposure and vulnerability found in this study. This method resembles the study of De Angeli et al., (2016), in which clusters are created using representative buildings. In this case, field observations from drones and services like Mapillary can be combined to create representative villages or towns.

Finally, the other sources of uncertainty accompanied by the damage estimation need to be further studied. Although they do not directly relate to the results of the exposure estimation, the sensitivity analysis in this research confirms that parameters such as floodwater characteristics, maximum damage values, and the applied damage curves have a significant effect on the total flood damage. To validate the water depth estimation, the effects of using a coarser resolution SRTM DEM in surface water interpolation should be tested. Preferably,

https://doi.org/10.5194/nhess-2020-417
Preprint. Discussion started: 15 January 2021

validation data from hydraulic models is used that corresponds to the flood event that is extracted from satellite imagery. This way, differences due to discharge uncertainties are limited. Also, the aggregation of damage curves based on building material could yield uncertainties in the resulting flood vulnerability. For a more accurate appropriation of the damage susceptibility, individual building types could be subjected to detailed survey studies that include historic flood events and damage with the corresponding building material.

5 Conclusions and outlook

The purpose of this research was to create a flood damage model based on the automated recognition of buildings and their characteristics through UAV image processing. By doing so, improvements on the exposure and vulnerability component of flood damage assessments were assessed and evaluated by comparing this new approach to a conventional one based on pixel-based information. The two flood damage models were applied in a rural and flood-prone area in Southern Malawi, with a building stock consisting of mostly semi-permanent structures structures.

In terms of direct structural damage considering the replacement costs of buildings in the study area, the flood damage based on homogenous land-use pixels is about 50% higher than the object-based approach (15k € vs 10k €). The calculation is found to be most sensitive to the damage curve that is used, with a sensitivity value (highest divided by lowest estimate) of 1.71 and 1.90. However, uncertainty in building exposure still results in sensitivities of 1.43 for a pixel-based approach and 1.21 for an object-based approach. This illustrates that accurate information on exposure is essential in accurately estimating potential flood damage.

The effects of including high-resolution elevation information in the OBIA were examined by including a height threshold for classified objects. Individual F1-scores of the object-based classification were improved from 0.89 to 0.90 for metal-roofed buildings and 0.53 to 0.72 for thatch-roofed buildings. These results show that the integration of accurate elevation data can improve standard classification schemes based solely on spectral bands. The relative error on the area of the detected buildings tends to be lower for larger buildings and buildings with a clear spectral difference with the surrounding area. The water depth, derived by interpolating the surface water boundaries of a remotely sensed flood extent, deviated on average 0.73 meters from a hydraulic model for a maximum water depth of approximately 3 meters. This validation was conducted for a subset of the case study river using a high-resolution DSM.

Based on the results of this study we find that the primary utility of high-resolution UAV imagery in flood damage assessment is to spatially locate buildings in inundated areas and retrieve their characteristics by creating typologies in combination with local observations. These characteristics can be used to apply damage curves that represent the local building stock instead of using aggregated information that implies homogeneous land cover for large regions. Furthermore, the number of buildings and their respective area and occupancy type can be derived to estimate flood damage more precisely. This improvement in data availability has the potential to aid humanitarian decision-makers in choosing appropriate policies with regard to flood protection or determining threshold levels for effective early-action measures in the case of flooding.

https://doi.org/10.5194/nhess-2020-417
Preprint. Discussion started: 15 January 2021

Natural Hazards and Earth System Sciences
Discussions

Data availability.

This work relied on data which are available upon request from the providers cited in Sects. 2 and 3.

Author contributions.

LW, HdM, MdR, AC and MvdH conceived the study. LW developed the theoretical framework and methodology with supervision from HdM, MdR, AC and MvdH. AK assisted in extracting and processing SAR data and helped LW carry out the inundation modelling. LW analysed the data and prepared the draft, with all co-authors providing critical feedback and helping shape the analysis and manuscript.

Competing interests.

The authors declare that they have no conflict of interest

Acknowledgements.

The authors would like to thank the Jurg Wilbrink (510) and Gumbi Gumbi and Simon Tembo from the Malawi Red Cross Society data team for obtaining the UAV data and Thirza Teule for collecting the essential field observations. The first and second European Civil Protection and Humanitarian Aid Operations (ECHO) program on resilience building in Malawi financed the UAV mission. Anaïs Couasnon acknowledges support from the Dutch Research Council (NWO) (VIDI; grant no. 016.161.324).

References

Ai, J., Zhang, C., Chen, L., and Li, D.: Mapping Annual Land Use and Land Cover Changes in the Yangtze Estuary Region Using an Object-Based Classification Framework and Landsat Time Series Data, Sustainability, 12(2), https://doi.org/10.3390/su12020659, 2020.

Alam, A., Bhat, M. S., Farooq, H., Ahmad, B., Ahmad, S., and Sheikh, A. H.: Flood risk assessment of Srinagar city in Jammu and Kashmir, India, International Journal of Disaster Resilience in the Built Environment, 9(2), 114–129, https://doi.org/10.1108/IJDRBE-02-2017-0012, 2018.

Amirebrahimi, S., Rajabifard, A., Mendis, P., and Ngo, T.: A framework for a microscale flood damage assessment and visualization for a building using BIM–GIS integration, Int. J. Digit. Earth., 9(4), 363–386, https://doi.org/10.1080/17538947.2015.1034201, 2016.

Belgiu, M., and Drăguţ, L.: Comparing supervised and unsupervised multiresolution segmentation approaches for extracting buildings from very high resolution imagery, Isprs. J. Photogramm., 96, 67–75, https://doi.org/10.1016/j.isprsjprs.2014.07.002, 2014.

Blanco-Vogt, Á., Haala, N., and Schanze, J.: Building parameters extraction from remote-sensing data and GIS analysis for the derivation of a building taxonomy of settlements – a contribution to flood building susceptibility assessment, International Journal of Image and Data Fusion, 6(1), 22–41, https://doi.org/10.1080/19479832.2014.926296, 2015.

Blaschke, T.: Object based image analysis for remote sensing, Isprs. J. Photogramm., 65(1), 2–16, https://doi.org/10.1016/j.isprsjprs.2009.06.004, 2010.

Budiyono, Y., Aerts, J., Brinkman, J., Marfai, M. A., and Ward, P.: Flood risk assessment for delta mega-cities: A case study of Jakarta. Nat. Hazards, 75(1), 389–413, https://doi.org/10.1007/s11069-014-1327-9, 2015.

https://doi.org/10.5194/nhess-2020-417
Preprint. Discussion started: 15 January 2021

Cian, F., Marconcini, M., Ceccato, P., and Giupponi, C.: Flood depth estimation by means of high-resolution SAR images and lidar data, Nat. Hazards Earth Sys., 18(11), 3063–3084. https://doi.org/10.5194/nhess-18-3063-2018, 2018.

CIESIN.: Facebook Connectivity Lab and Center for International Earth Science Information Network. High Resolution Settlement Layer (HRSL), Center for International Earth Science Information Network, https://www.ciesin.columbia.edu/data/hrsl/, 2016.

Cohen, J.: A Coefficient of Agreement for Nominal Scales. Educ. Psychol. Meas., 20(1), 37–46, https://doi.org/10.1177/001316446002000104, 1960.

Cohen, S., Brakenridge, G. R., Kettner, A., Bates, B., Nelson, J., McDonald, R., Huang, Y.-F., Munasinghe, D., and Zhang, J.: Estimating Floodwater Depths from Flood Inundation Maps and Topography, J. Am. Water Resour. As., 54(4), 847–858. https://doi.org/10.1111/1752-1688.12609, 2018.

Copier, W., de Ruiter, M. C., de Moel, H., Couasnon, A. A., & Teklesadik, A.: The impact of drone data on hydraulic modelling – A case study for an area in Malawi, Vrije Universiteit Amsterdam, 2019

De Angeli, S., Dell'Acqua, F., and Trasforini, E.: Application of an Earth-Observation-based building exposure mapping tool for flood damage assessment, E3S Web of Conferences, 7, 05001, https://doi.org/10.1051/e3sconf/20160705001, 2016.

de Moel, H., and Aerts, J. C. J. H.: Effect of uncertainty in land use, damage models and inundation depth on flood damage estimates, Nat. Hazards, 58(1), 407–425, https://doi.org/10.1007/s11069-010-9675-6, 2011.

de Moel, H., Asselman, N. E. M., & Aerts, J. C. J. H.: Uncertainty and sensitivity analysis of coastal flood damage estimates in the west of the Netherlands, Nat. Hazard Earth Sys., 12(4), 1045–1058. https://doi.org/10.5194/nhess-12-1045-2012, 2012.

Díaz-Delgado, C., and Gaytán Iniestra, J.: Flood Risk Assessment in Humanitarian Logistics Process Design, J. Appl. Res. Technol., 12(5), 976–984, https://doi.org/10.1016/S1665-6423(14)70604-2, 2014.

Englhardt, J., Moel, H. de, Huyck, C. K., Ruiter, M. C. de, Aerts, J. C. J. H., and Ward, P. J.: Enhancement of large-scale flood risk assessments using building-material-based vulnerability curves for an object-based approach in urban and rural areas, Nat. Hazards Earth Sys., 19(8), 1703–1722, https://doi.org/10.5194/nhess-19-1703-2019, 2019.

Farr, T. G., & Kobrick, M.: Shuttle radar topography mission produces a wealth of data. Eos, Transactions American Geophysical Union, 81(48), 583. https://doi.org/10.1029/EO081i048p00583, 2000.

Fekete, A.: Spatial disaster vulnerability and risk assessments: Challenges in their quality and acceptance, Nat. Hazards, 61(3), 1161–1178, https://doi.org/10.1007/s11069-011-9973-7, 2012.

Government of Malawi.: 2015 Floods Post Disaster Needs Assessment Report—Malawi, Government of Malawi, https://reliefweb.int/report/malawi/malawi-2015-floods-post-disaster-needs-assessment-report, 2015.

Grizonnet, M., Michel, J., Poughon, V., Inglada, J., Savinaud, M., and Cresson, R.: Orfeo ToolBox: Open source processing of remote sensing images, Open Geospatial Data, Software and Standards, 2(1), 15, https://doi.org/10.1186/s40965-017-0031-6, 2017.

Hydrologic Engineering Center: HEC-RAS, River Analysis System User's Manual, Version 3·1. Davis: California, 1998.

IFRC.: Malawi Floods: Emergency Plan of Action (EPoA) (p. 15) [Situation Report], International Federation of Red Cross And Red Crescent Societies, file:///C:/Users/Woute/Downloads/MDRMW014do%20(2).pdf, 2019.

Jones, B.: Managing Post-Disaster Needs Assessments (PDNA), Managing Post-Disaster Needs Assessments (PDNA), World Bank, Washington, DC., EAP DRM Knowledge Notes; No. 19, 8, 2010.

https://doi.org/10.5194/nhess-2020-417
Preprint. Discussion started: 15 January 2021

Jongman, B., Kreibich, H., Apel, H., Barredo, J. I., Bates, P. D., Feyen, L., Gericke, A., Neal, J., Aerts, J. C. J. H., and Ward, P. J.: Comparative flood damage model assessment: Towards a European approach, Nat. Hazards Earth Sys., 12, 3733–3752, https://doi.org/10.5194/nhess-12-3733-2012, 2012.

Ke, Q., Jonkman, S. N., Van Gelder, P. H. a. J. M., and Rijcken, T.: Flood damage estimation for downtown Shanghai sensitivity analysis. Conference of the International Society for Integrated Disaster Risk Management IDRiM 2012, Authors Version: International Society for Integrated Disaster Risk Management, Beijing, China, https://repository.tudelft.nl/islandora/object/uuid%3Abf75cdab-8a0d-4dbf-ae8e-61f59d3e5d86, 2012.

Klemas, V. V.: Coastal and Environmental Remote Sensing from Unmanned Aerial Vehicles: An Overview, J. Coastal Res., 31(5), 1260–1267, https://doi.org/10.2112/JCOASTRES-D-15-00005.1, 2015.

Koks, E. E., Bočkarjova, M., Moel, H. de, and Aerts, J. C. J. H.: Integrated Direct and Indirect Flood Risk Modeling: Development and Sensitivity Analysis, Risk Analysis, 35(5), 882–900, https://doi.org/10.1111/risa.12300, 2015.

Ma, L., Li, M., Ma, X., Cheng, L., Du, P., and Liu, Y.: A review of supervised object-based land-cover image classification, Isprs. J. Photogramm., 130, 277–293, https://doi.org/10.1016/j.isprsjprs.2017.06.001, 2017.

Maiti, S.: Defining a Flood Risk Assessment Procedure using Community Based Approach with Integration of Remote Sensing and GIS, International Institute for Geo-information Science and Earth Observation, 2007.

Malawi Statistical Office: Fourth Integrated Household Survey (IHS4) 2016-2017, Ministry of Economic Planning and Development (MoEPD), 2017.

Mallupattu, P. K., and Sreenivasula Reddy, J. R.: Analysis of Land Use/Land Cover Changes Using Remote Sensing Data and GIS at an Urban Area, Tirupati, India, The Scientific World Journal, 2013, e268623, https://doi.org/10.1155/2013/268623, 2013.

Merz, B., Kreibich, H., Schwarze, R., and Thieken, A.: Review article "Assessment of economic flood damage.", Nat. Hazards Earth Sys., 10(8), 1697–1724, https://doi.org/10.5194/nhess-10-1697-2010, 2010.

Merz, B., Kreibich, H., Thieken, A., and Schmidtke, R.: Estimation uncertainty of direct monetary flood damage to buildings. Nat. Hazards Earth Sys., 4(1), 153–163, https://doi.org/10.5194/nhess-4-153-2004, 2004.

Michel, J., Youssefi, D., and Grizonnet, M.: Stable Mean-Shift Algorithm and Its Application to the Segmentation of Arbitrarily Large Remote Sensing Images, IEEE T. Geosci. Remote, 53(2), 952–964, https://doi.org/10.1109/TGRS.2014.2330857, 2015.

Mountrakis, G., Im, J., and Ogole, C.: Support vector machines in remote sensing: A review, Isprs. J. Photogramm., 66(3), 247–259, https://doi.org/10.1016/j.isprsjprs.2010.11.001, 2011.

Mouratidis, A., & Sarti, F.: Flash-Flood Monitoring and Damage Assessment with SAR Data: Issues and Future Challenges for Earth Observation from Space Sustained by Case Studies from the Balkans and Eastern Europe, In J. M. Krisp, L. Meng, R. Pail, & U. Stilla (Eds.), Earth Observation of Global Changes (EOGC) (pp. 125–136), Springer Berlin Heidelberg. https://doi.org/10.1007/978-3-642-32714-8_8, 2013.

Murnane, R. J., Daniell, J. E., Schäfer, A. M., Ward, P. J., Winsemius, H. C., Simpson, A., Tijssen, A., and Toro, J.: Future scenarios for earthquake and flood risk in Eastern Europe and Central Asia, Earth's Future, 5(7), 693–714, https://doi.org/10.1002/2016EF000481, 2017.

© OpenStreetMap contributors.: OpenStreetMap. OpenStreetMap, from https://www.openstreetmap.org, retrieved July 2 2019.

Ruiter, M. C. D., Ward, P. J., Daniell, J. E., and Aerts, J. C. J. H.: Review Article: A comparison of flood and earthquake vulnerability assessment indicators, Nat. Hazards Earth Sys., 17(7), 1231–1251, https://doi.org/10.5194/nhess-17-1231-2017, 2017.

https://doi.org/10.5194/nhess-2020-417
Preprint. Discussion started: 15 January 2021

Natural Hazards and Earth System Sciences
Discussions

Shen, X., Wang, D., Mao, K., Anagnostou, E., and Hong, Y.: Inundation Extent Mapping by Synthetic Aperture Radar: A Review., Remote Sens., 11(7), 879, https://doi.org/10.3390/rs11070879, 2019.

SNAP: European Space Agency Sentinel Application Platform v6.0. ESA. http://step.esa.int, 2019.

Teule, T., Couasnon, A., Bischiniotis, K., Blasch, J., and van den Homberg, M.: Towards improving a national flood early warning system with global ensemble flood predictions and local knowledge; a case study on the Lower Shire Valley in Malawi., EGU General Assembly 2020,, EGU2020-507, https://doi.org/10.5194/egusphere-egu2020-507, 2019

UNDRR: Global Assessment Report on Disaster Risk Reduction. United Nation office of Disaster Risk Reduction, 2019.

van den Homberg, M. J. C., Wilbrink, J., Crince, A., Kersbergen, D., Gumbi, G., Tembo, S., & Lemmens, R.: Combining UAV imagery and geospatial data to improve characterization of rural water points in Malawi, Int. J. Geo-inf., Special Issue “Measuring and Monitoring Progress towards SDGs by Integrating Geospatial and Statistical Information.”, 2020.

van den Homberg, M., & Susha, I.: Characterizing Data Ecosystems to Support Official Statistics with Open Mapping Data for Reporting on Sustainable Development Goals, ISPRS Int. J. Geo-Inf., 7(12), 456. https://doi.org/10.3390/ijgi7120456, 2018.

W., C., de Ruiter, M. C., de Moel, H., Couasnon, A. A., and Teklesadik, A.: The impact of drone data on hydraulic modelling – A case study for an area in Malawi, Vrije Universiteit Amsterdam, 2019.

Wagenaar, D. J., Bruijn, K. M. de, Bouwer, L. M., and de Moel, H.: Uncertainty in flood damage estimates and its potential effect on investment decisions, Nat. Hazards Earth Sys., 16(1), 1–14, https://doi.org/10.5194/nhess-16-1-2016, 2016.

Xu, L., Jing, W., Song, H., and Chen, G.: High-Resolution Remote Sensing Image Change Detection Combined With Pixel-Level and Object-Level, IEEE Access, 7, 78909–78918, https://doi.org/10.1109/ACCESS.2019.2922839, 2019.

Ye, S., Pontius, R. G., and Rakshit, R.: A review of accuracy assessment for object-based image analysis: From per-pixel to per-polygon approaches, Isprs. J. Photogramm., 141, 137–147. https://doi.org/10.1016/j.isprsjprs.2018.04.002, 2018.